Structural and magnetic properties of zinc ferrite thin films irradiated by 90keV neon ions

E.V. Gafton, G. Bulai, O.F. Caltun, S. Cervera, Stéphane Macé, Martino Trassinelli, Sébastien Steydli, Dominique Vernhet

Structural and magnetic properties of zinc ferrite thin films irradiated by 90 keV neon ions

E.V. Gafton[a,b,*], G. Bulai[a], O.F. Caltun[a], S. Cervera[b], S. Macé[b], M. Trassinelli[b], S. Steydli[b], D. Vernhet[b]

[a]*Alexandru Ioan Cuza University, Faculty of Physics, 11 Carol I Blv, Iasi 700506, Romania*

[b]*Institut des NanoSciences de Paris, CNRS-UMR 7588, Sorbonne Universités, UPMC Univ Paris 06, 75005, Paris, France*

*Corresponding author: Tel./ fax: +40232201174
E-mail addresses: elena.gafton@insp.jussieu.fr(E.V. Gafton),caltun@uaic.ro (O.F. Caltun), dominique.vernhet@insp.jussieu.fr (D. Vernhet)

Graphical abstract

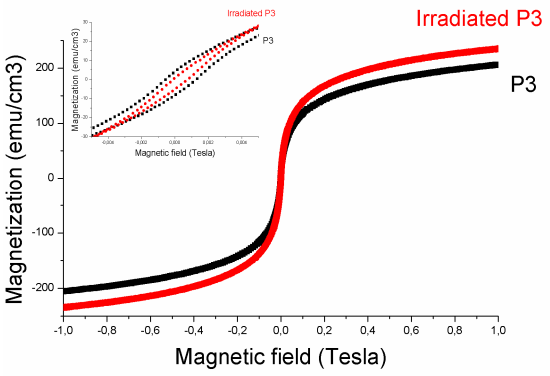

Highlights

- Effect of different ion beam fluences on zinc ferrite thin films structure was investigated
- First reported results on zinc ferrite thin films irradiated with slow highly charged ions
- Increased magnetization was observed for samples irradiated even at low fluence
- Measurements of blocking temperature of thin films before and after irradiation

Abstract

The effects of 90 keV neon beam irradiation on the structure and magnetic properties of zinc ferrite thin films have been investigated through several methods, namely, X-ray diffraction technique, Vibrating Sample and SQUID magnetometers. Beforehand, the pristine have also been characterized using profilometry and microscopy techniques. In particular single-phase formation of the thin films

deposited on monocrystalline Si (111) substrate by pulsed laser deposition technique was confirmed. Crystal lattice, coercivity, saturation magnetization have been studied for the first time, as a function of ion penetration depth and irradiation fluence. The chemical composition and the crystallinity of the films are not affected with the ion impact acting as a mechanical stress relief. On the contrary, both magnetization and coercivity are sensitive to Ne^{q+} ion irradiation and exhibit different behaviours depending on the ion fluence range.

Keywords: spinel; zinc ferrite; thin film; PLD; ion irradiation;

1. INTRODUCTION

Zinc ferrite, $ZnFe_2O_4$, in its bulk form exhibits normal spinel structure having all the Zn^{2+} on A-site and all the Fe^{3+} ions on B-site [1]. Depending on the type of cations occupying the A-site and the B-site, these spinel-type ferrites may show different magnetic behaviour [2]. In fact, their magnetic properties can be systematically varied by changing the identity or partial substitution of the divalent Zn^{2+}cation, while maintaining the basic crystal structure. Zn ferrite, which is a paramagnet at room temperature in bulk form, has been found to have magnetic order at room temperature in thin films [3]. Such zinc ferrite systems with nanometer particle size are generally obtained by non-equilibrium processes like by solgel self-combustion [4] for obtaining ultrafine particles, or by pulsed laser deposition (PLD) [5]. Depending on deposition parameters, Yamamoto et *al.*[6]identified two possible causes for the origin of magnetism in zinc ferrite thin films: i) spin frustration resulting from the competition of antiferromagnetic interaction between A-B and B-B site iron ions, and ii) random oxygen deficiency.

Another way to modify material magnetic properties is the use of heavy ion irradiation either in bulk [7] or in thin films [8 - 17]. Number of investigations have been done, like for instance with GeV multicharged heavy ions (Kr, Xe, Pb, U) going through bulk zinc ferrite (synthesized by typical solid state chemistry) where it leads to cation redistribution and increases the magnetization of the system [7]. Similar effect of cation redistribution was observed in zinc ferrite nanoparticles when irradiated

with 100 MeV oxygen beam but in this case the magnetization of irradiated samples was found to decrease [18-20]. The reduction in magnetization after the irradiation in the specimen is attributed to the decrease in cation inversion and increase in canting angle after irradiation [19]. On the other hand, only sparse studies have been performed so far with low-velocity charged ions regarding the possible induced modifications of material magnetic properties. Most of the investigations have been done with mono-charged ions [8-16]. Of course for a given target, various factors will affect the material properties when irradiated by slow charged ions, such as: ion species, fluence of the irradiation, besides the incident ion energy, and will be also dependent on the initial target structure. Considering thin films, very recently, Trassinelli et *al.* [17, 21] demonstrated that slow ion impact (Ne^{9+} at 90 keV) can lead to very promising magnetic modification of giant magnetocaloric material such as MnAs deposited on GaAs substrate. Indeed, the slow highly-charged ions induce defects that facilitate the two phases' nucleation in the first-order magneto-structural MnAs transition, with a consequent suppression of the thermal hysteresis without any significant perturbation on the other structural and magnetic properties. In particular, the irradiated film keeps the giant magnetocaloric effect (i.e. its large refrigerant power) at room temperature opening new perspectives on magnetic refrigeration technology for everyday use.

In this paper, we present results on the influence of irradiation conditions on the properties of zinc ferrite thin films in order to understand the magnetization and the coercive field modifications. More precisely, changes of the zinc ferrite film properties after irradiation, namely coercivity, saturation magnetization, crystal lattice etc., were studied for the first time as a function of the ion penetration depth and the irradiation fluence of slow $Ne^{8+}$and Ne^{9+} charged ions with a kinetic energy of 90 keV. Different samples obtained by the same synthesis method have been studied. This investigation not only increases the applicability of zinc ferrites but also elucidates the interaction of slow charged ions with magnetic nanomaterials. For the best of our knowledge there are no reported results describing the influence of slow charged ions on zinc ferrite thin films obtained by PLD.

2. EXPERIMENTAL CONDITIONS AND METHODS

2.1 SYNTHESIS

A series of zinc ferrite thin films exhibiting magnetic order were grown under controlled conditions at room temperature on Si (111) substrates by PLD [22, 23].The thin films were deposited using a stoichiometric zinc ferrite target [24] as source material (referred as "PLD target" in what follows). The second harmonic of a Nd: YAG laser (532 nm) with a pulse duration of 10 ns in 10 Hz repetition rate was focused on the target surface at 45° incidence angle. All the samples were obtained at room temperature in a background pressure of $3x10^{-2}$ Torr, for 1h deposition time with a deposition fluence of 2.5 J/cm^2. The 4 cm distance between the zinc ferrite target and silicon substrate was kept constant. The crystallinity of samples was assured by subsequent annealing at 700°C in vacuum, with a heating rate of 100°C/h, and the samples then underwent free cooling still in vacuum.

Structural and magnetic properties of these zinc ferrites thin films were studied before and after being irradiated by 90 keV neon beams.

2.2THIN FILM CHARACTERIZATION

Investigation on film thickness and deposition rate was performed on a fractured as-deposited sample by using a mechanical profilometer Dektak 150 Veeco for long-range determination in the step zone(accuracy: about 2.5 nm). Complementary a scanning electron microscope (SEM) Hitachi S3400-N was implemented for obtaining cross-sectional images. The surfaces of the samples were covered with a 15 nm gold layer, to avoid charging during SEM measurements. Film surface morphology was examined with an atomic force microscope (AFM) Digital Instrument DI3100. Topographic AFM measurements were performed in tapping mode at constant working amplitude (set point).

Measurements on the microstructure of the PLD target and of the thin films before and after the irradiation sequences were performed using X-ray diffraction (XRD) by a Rigaku Smartlab diffractometer with a copper rotating anode, generating Cu $K_{\alpha 1}$ radiation, equipped with a Ge (220) 2 reflections' monochromator, and operating at 45 kV and 200 mA (9kW). This is a classical method for determining the structural properties such as grain sizes, crystal lattice parameters, etc. XRD patterns were recorded in the 10–80°2θ range. The crystallite size was mirrored by the broadening of the diffraction peaks. The size of the crystallites was calculated from the full width at half-maximum of the diffraction peaks and the lattice parameter was estimated from the positions of the $ZnFe_2O_4$(311) diffraction lines. The crystallite size *D* for the as-deposited sample was estimated using Scherer's equation $D = k \cdot \lambda / \beta \cdot cos\theta$ [25].

The magnetic properties of the thin films were studied in fields of up to 1 T using a vibrating sample magnetometer Quantum Design PPMS 9T. We recorded the magnetization as a function of the applied field at room temperatures (RT) and at lower temperatures (200K, 100K and 10 K) for the pristine and irradiated specimen in order to observe the possible changes in the magnetic properties of the system under investigation. Further, thermal magnetic measurements in the temperature range from 4 to 310 K, in zero-field cooled (ZFC) and field cooled (FC) mode were carried out to investigate magnetization dependence on temperature and determine the blocking temperature of each sample. The sample temperature dependency of magnetization was obtained using a SQUID magnetometer (Quantum Design MPMS-XL). The measurement procedure was the following:

i. each sample was initially brought to 300 K with H = 0;
ii. the sample was cooled down to 4 K and then a magnetic field of H = 1 T was applied;
iii. the magnetic moment was continuously recorded during the temperature variation from 4 to 310 K, and then back to 4 K, with a sweeping rate of ±2 K/min.

2.3IRRADIATION PROCESS

The charged ions used in our experiments are produced at the SIMPA (Source d'Ions Multichargés de Paris = Paris highly-charged ion source) [26] facility. It consists of a Pantechnick Supernanogan type Electron Cyclotron Resonance (ECR) ion source equipped with a full permanent magnet and coupled to a dedicated beam line. The ion source can produce intense beams of highly-charged ions such as O^{5+}, Ne^{9+}, Ar^{16+}, Kr^{21+}, Xe^{26+}, etc. After the extraction from the plasma of the ECR ion source, the ion beam is selected in charge and mass by an auto-focusing magnetic dipole. With a series of magnetic and electric lenses and steerers, the ion beam is guided to the collision chamber where different samples are placed. In our case, we use Ne^{8+} and Ne^{9+}ion beams with kinetic energy of 90 keV (4.5 keV/u). Note that the charge state does not influence here the total energy since the contribution of the ion potential energy is negligible compared to their kinetic energy. The samples were irradiated under 30° incidence angle relative to the sample surface and at different fluences. The ion current was kept between 0.4 μA and 0.6 μA. The evaluation of the implantation range and damage distribution induced by the interaction between the ion beam and the zinc ferrite thin film were obtained using SRIM software [27]. The result of the simulation, presented in Figure 1, indicates an ion penetration depth covering approximately the entire thickness of the Zn ferrite film. The ion fluence used ranges from 3×10^{11} to 3×10^{14} ions/cm^2 (± 50%) and was estimated by a CCD camera that permanently monitored the position of the beam onto the samples. In addition, during this experimental campaign the shape of the beam was controlled for the first time by an advanced Faraday cup arrays (FCA) [28, 29] that can be inserted (and retracted when the samples are placed) inside the collision chamber. The schematic set-up is presented in Figure 2. It is worth mentioning that the uncertainty of 50% on the fluence has no crucial impact on the measurements reported and discussed in this paper.

The samples obtained in similar deposition and annealing conditions, denoted P_i (i = 1, 2, 3, 4), were irradiated under parameters presented in Table 1.

3. RESULTS AND DISCUSSIONS

3.1 CHARACTERISATION OF PRISTINE SAMPLES

3.1.1 Morphology and structure

The thickness of the zinc ferrite films obtained by profilometry measurements was approximately 250 nm. Local variations up to 20% suggest a grain type non-uniform surface. This mean value corresponds to a deposition rate of 4 nm/min [22] and is confirmed by SEM measurement. In Figure 3 is presented the cross section corresponding to as-deposited sample P1. The surface of the thin films exhibited distinct three-dimensional island-like grains that demonstrated considerable surface roughness. The droplet contamination usually associated with the PLD process [30] is present and occurs due to high repetition rate of the laser pulses [31] even if low laser energies and relatively large target substrate distance are used.

AFM imaging confirms the non-uniformity of the film thickness. Room-temperature atomic force micrographs taken for the as-deposited, annealed and irradiated zinc ferrite films shows no major differences concerning the average grain sizes and rugosity, values presented in Table 1. A mean value of 25 nm (± 1 5 nm) is estimated for the grain sizes in the annealed zinc ferrite thin film P1for example. Ex situ surface roughness measurement by AFM indicates that the difference between the lowest and highest points, R_{p-p}, on the surface is 10 nm for all samples. The surface of the P1 epilayer presented in Figure 4 (a) (32) is dense and exhibits small circular surface grains. The grains are non-uniform and the granule diameters range from 25 to 40 nm, corroborating the SEM observations.

Clear patterns with peaks corresponding to zinc ferrite cubic spinel phase and to Si (111) substrate were observed in the XRD data. The width of the peaks is slightly narrow and less intense than for the PLD target. The annealing treatment determines a nucleation process and polycrystalline structured films. Figure 5 shows as example for P3 sample a zoom of the XRD pattern of $ZnFe_2O_4$ thin film prepared by laser ablation method before and after the annealing treatment. The XRD pattern of the polycrystalline PLD target is also presented for comparison. Qualitative phase identification was performed using 89-1009 ICDD [32] card of zinc ferrite. As-deposited thin films patterns suggest an

amorphous structure with isolated polycrystalline islands [22]. A large discrepancy appears between the crystallite sizes estimated from XRD and average grain dimension determined from AFM images in the present work. It seems that irregular shape of grains, as observed in AFM, does not allow using Scherrer's formula for size determination, but this may not be true since XRD pattern comes from reflections of crystallites not grains [33]. It means that crystallite size can be reliably measured by XRD, while AFM provides measurements of grain size, which is a combination of several crystallites [34, 35].

Table 1 presents a summary of characteristics (lattice parameter *a*, crystallite sizes *D*, AFM grain sizes and R_{p-p}) after annealing treatment of the samples obtained by PLD as well as for the PLD target.

The crystallite size *D* for the as-deposited samples which are a mix of amorphous and crystalline phase is estimated to be 4 nm (± 1.2 nm), much smaller than the 20 nm (± 0.3 nm) for the PLD target material. After the annealing process, the crystallite size increases to 12 nm (±0.2 nm). The increase of crystallite size may due to cation redistribution in spinel interstitial, at high annealing temperature Zn^{2+} and Fe^{3+} cations tend to rearrange themselves in tetrahedral and octahedral sites [37] The crystallite size value corresponding to annealed thin film is in good agreement with previous studies on zinc ferrite thin films [36] obtained by RF sputtering. Moreover, the lattice parameter *a* of $ZnFe_2O_4$ P3 thermally annealed thin film is estimated to be 8.42 Å (±0.07 Å) from the positions of diffraction lines corresponding to (311) planes. This value is slightly smaller than the reference value reported in the ICDD cards (89-1009), i.e., 8.44 Å (± 0.02 Å) for the lattice parameter of $ZnFe_2O_4$ (franklinite), due to cation redistribution during the growth process. Lattice parameter of annealed samples in the limit of the experimental errors is close to the PLD target material value of 8.44 Å (± 0.07 Å).

3.1.2 Magnetic properties

Data on field dependence of magnetization, presented in Figure 6 for sample P3, provide a strong evidence for the mix of superparamagnetism and ferrimagnetism of the grains ranging in between tens of nanometers. The M (H) curves are not saturated at 1 T magnetic field and the

magnetization value, at 300 K for an applied field of 1 T, ranges between 40 and 165 emu/cm^3. This is comparable with 55 emu/cm^3, also measured at 300 K, found by Timopheev*et al.* [37] for zinc ferrite thin films deposited by PLD. The magnetic hysteresis loops are clearly observed in the low-field ranges, for all samples and in particular for P3 sample, as shown in the inset of Figure 6.

The result of zero-field-cooled (ZFC) and field cooled (FC) for $ZnFe_2O_4$ sample P3 is presented in Figure 7. Closed and open circles indicate the magnetization values in ZFC and FC processes, respectively. The ZFC-FC curves separation at lower temperature is known as a high field irreversibility ($M_{FC}>M_{ZFC}$) behavior below a certain temperature.

Different magnetization and T_B values of pristine samples can be correlated by different degree of cation distribution occurred after ablation and thermal treatment of samples [40].

3.2 CHARACTERISATION OF IRRADIATED SAMPLES

3.2.1 Morphology and structure

The irradiation bombardment for each angle and fluence does not result in any significant change in grains dimension compared with unirradiated zinc ferrite thin film. Well defined topographic data of irradiated samples P2, P3, P4 is presented in Figure 4 (b). We note only that the film surface of irradiated samples consists of numerous tiny bumps, with a constant R_{p-p} (10 nm) compared to non-irradiated film. A light smoothness of the samples surfaces could be induced by the effect of the thermal processes that take place during irradiation.

The XRD data show that the crystallinity is not perturbed after irradiation. Values reported in Table 1, estimated from 311 peaks for all the samples indicate that the irradiation did not affect the structure of the thin films. Small alteration of the structure was observed from the decrease of (400) reflection peak after irradiation. It should be noted that the lattice constant for the thin film obtained by the laser ablation method contains some uncertainties because of the broadness of the diffraction lines.

Similarly, J.P. Singh and coworkers also found an increase of the lattice parameter of 10 nm for particle sized zinc ferrite from 8.21 Å to 8.29 Å, but they used higher energy beam for irradiating the samples, respectively 100 MeV O-beam [19]. They concluded that the irradiation process lead to destruction of crystalline structure. Accordingly, it means that at low energy, the 90 keV ion irradiation leads as well to the destruction of the crystalline structure.

3.2.2 Magnetic properties

In Table 1 we reported the magnetization value with an applied field of 1 T for the different samples. As we can observe, after irradiation, the magnetization is systematically higher than in pristine samples. A similar behavior has been observed by Studer *et al.* when analyzing 65 µm thin $ZnFe_2O_4$ disks irradiated with different fluences of tens of MeV/a Kr, Xe, Pb, U heavy ions [7]. They attributed this increase to a subsequent distribution of ferric ions over tetrahedral and octahedral sites induced after irradiation in zones extending around heavy ions trajectories. An increase of the magnetization has also been observed in 30-60 nm zinc ferrites and other nanocrystalline ferrites irradiated by 200 MeV Ag^{15+} [42-45]. The analog magnetization increasing after irradiation in our case signifies that also low energy irradiations can lead to rearrangement of metallic cations inside the thin films. A quantitative analysis to rely the magnetization increasing and the received fluence is unfortunately not possible. As we can see in Table 1 the increasing of the magnetization ranges between 5 and 30% with no correlation on the received fluence. Even if structurally similar, the samples have in fact a too different magnetization before irradiation to extract accurate information on the effect of the ion bombardment.

Large difference on the magnetic hysteresis cycles is noticeable between the pristine and the irradiated sample, presented in the inset of Figure 6. A global increase of the maximum value of the coercive field is noticeable at room temperature for all samples as we can see in Table 1, except sample P3 for which we can consider the 0.7 kA/m coercivity negligible compared to other samples. Studies on other ferrites nanoparticles irradiated by swift heavy ions also indicated a small increase of

the coercivity [42-45] for samples where the irradiation lead to crystal growth, cation redistribution and surface modifications. Singh *et al.* (39) reported in a similar study on size dependent features of swift heavy ion irradiation in nanoparticles zinc ferrite systems. They observed that structural properties of the samples with smaller particle size are more sensitive towards irradiation. They also noticed that the coercive field is unchanged when small particle sized samples are irradiated but decreases for larger particle sized samples, which is the opposite effect than the irradiation with slow ions. We can conclude that for the coercivity of small particle size samples, swift and low velocity ions have similar effect. Similarly than for the magnetization, no quantitative dependency on the fluence can be extracted from our data.

Although all irradiated films show quite similar crystallographic behaviours and crystal ion configurations compared to the corresponding non-irradiated films, different magnetic behaviours appear, including the irreversible point in magnetization-temperature curve between zero-field-cooling and field-cooling process. This behaviour derives from the single magnetic domain structure of grains with several tens of nanometer size. Particle sizes, in the order of tens of nanometer derived from AFM studies, correspond to a single magnetic domain. Because single domain particles are hard to magnetize, a magnetic blocking point shows up. Information on the blocking temperature (T_B) in the present study was achieved from the ZFC curve maxima [46-47]. From Figure 7 curves, the ZFC and FC are almost overlapped above T_B, indicating the presence of the small sized particles [48]. The maximum of ZFC curve of the as-deposited zinc ferrite thin film P3 is located at T_B= 216 K, then M_{ZFC} strongly decreases since the superparamagnetic- ferromagnetic transition activates the anisotropy, which forces the magnetization along easy axis; the magnetic moments are thus randomly oriented. It is observed that this temperature is quite different for the nanosized crystalline system synthesized by different routes, in spite of having a similar particle size [49-50], more precisely, 8 nm particle size samples presented 30 K blocking temperature. The field cooled (FC) curves show a peculiar behavior with a decrease in the magnetization at very low temperature. These unusual magnetic properties are attributed to the inclusion of nonmagnetic zinc ions in ferrite nanocrystals,

which induces a magnetic disorder [51]. A shift of the blocking temperature of the irradiated samples from 216 K to 226 K is observed from the thermal magnetization curve.

Changes in the magnetization are linked to a partial inversion of the direct spinel phase [52]. A shift of the blocking temperature also toward higher values was observed in the case of 10 nm zinc ferrite nanoparticles [20] when irradiated by $5x10^{13}$ ions/cm^{2}100 MeV oxygen beams but also in other ferrite irradiated by 200 MeV Ag^{15+} beams [42-45]. To justify the irradiation-induced magnetization, it can be assumed that atomic displacements of Fe^{3+} cations at tetrahedral sites took place. Under irradiation, in a volume fraction of the samples, iron atoms undergo displacement from octahedral to tetrahedral sites of the spinel structure [53]. Implicitly, Zn^{2+} cations can move from tetrahedral to octahedral sites. Taking into account the high values of the magnetization measured in the irradiated samples, it is obvious that these displacements involve large concentrations of iron atoms. In our case, the broadness of the ZFC curves indicates a particle size distribution in the nanosystems and the slight shift of the maxima after the irradiation confirms that the low energy ion impact induces displacement of the cations.

5. CONCLUSIONS

Investigation on the behavior of structural and magnetic properties of Zn ferrite thin films irradiated by $Ne^{8+}$and Ne^{9+} ions at energy of 90 keV showed that this energy is sufficient to tailor the magnetic properties while the structure is not strongly modified by the bombardment. XRD analysis reveals that all zinc ferrite thin film samples obtained by PLD technique after the 700°C annealing process have single-phase cubic spinel structure and the particle size from AFM micrographs is in nanometers regime. XRD and AFM studies have shown that laser ablated zinc ferrite thin films do not exhibit significant morphology changes after irradiation with slow charged ions. Crystalline phase of this system is not significantly affected by the thermal treatment caused by the 90 keV neon beam. Irradiation does not affect the chemical composition of the films, but induces significant modifications

in magnetic properties. Both magnetization and coercive field are sensitive to Ne^{q+} ion irradiation and exhibit different behaviours depending on the ion fluence range. The observed change in the material magnetic properties is due to interaction of charged ions with the electron energy levels. The modifications of the magnetic properties could be explained by the effects related to the disordered cation arrangement induced by slow ion irradiation in agreement with previous works where high energy irradiation was used.

The number of displacement per atom calculated using SRIM software indicates that 90 keV Ne beams produce a density of displacement in 250 nm zinc ferrite target of $10^{22}/cm^3$.Calculated from 845/ion vacancies displacement multiplied by the fluence of Ne beam and divided by the target thickness, it is higher than in previous works where the density of displacement was $3.1x10^{18}$ for 100 MeV O^{7+} [20] and $1.4x10^{19}$ for 3.7 MeV Kr [7]. Except the case of the lightest oxygen projectiles, with the less induced displacement, we can conclude that for the coercivity and magnetization of small particle size samples, swift and low velocity ions have similar effect.

Further experiments will be performed also at low energy but using different ion species such as Ar^{q+}, or O^{q+} on same material system and also on different ferrite nanosystems, as MFe_2O_4, where M = Co, Ni, Mn in order to perform complementary investigations to elucidate the effect of slow charged ion impact with magnetic nanomaterials. Quantitative study of the magnetic characteristics change as function of the ion fluence will be done using different portion of the same sample.

Acknowledgements. This work was supported by the strategic grant POSDRU/159/1.5/S/137750, Project "Doctoral and Postdoctoral programs support for increased competitiveness in Exact Sciences research" co financed by the European Social Found within the Sectorial Operational Program Human Resources Development 2007 – 2013. This work was partially supported by French state funds managed by the ANR within the Investissements d'Avenir programme under reference ANR-11-IDEX-0004-02, and more specifically within the framework of the Cluster of Excellence MATISSE led by Sorbonne Universités.

Authors acknowledge S. Gurlui (LOASL) for providing PLD equipment, S. Tascu (RAMTECH) for SEM measurements, Loic Becerra (INSP) for profilometry indications, Emmanuelle Lacaze (INSP) for the AFM indications and Sarah Hidki (INSP) for the XRD measurements. VSM and SQUID facilities are part of Sorbonne Universités Platform. Authors acknowledge Emily Lamour, Christophe Prigent and Louis Bernard Carlsson for participation during irradiation experiments and fruitful discussions.

Bibliography

1. B. D. Cullity, "*Introduction to Magnetic Materials*", Addision Wesley, London, 1957

2. A. Hossain, H. Tabata, T. Kawai, *J. Magn. Magn.Mater*. **320** 1157–1162 (2008)

3. J. Joseph, R.B. Tangsali, V.P. Mahadevan Pillai, R.J. Choudhary, D.M. Phase, *Materials Research Bulletin* **61**475–480 (2015)

4. N. Rezlescu, E. Rezlescu, F. Tudorache, P.D. Popa,*RomanianReportsin Physics* **61** (2) 223-234 (2009)

5. O.F. Caltun, L.S. Hsu, *Journal of Optoelectronics and Advanced Materials* **9** (4)1155-1157 (2007)

6. Y. Yamamoto, H. Tanaka, T. Kawai,*Jpn. J. Appl. Phys.* **40** (2) L545 (2001)

7. F. Studer, Ch. Houpert, D. Groult, J. Yun Fan, A. Meftah, M. Toulemonde, *Nucl. Instrum. Methods B* **82**91-102 (1993)

8. C. Chappert, H. Bernas, J. Ferré, V. Kottler, J.P. Jamet, Y. Chen, E. Cambril, T. Devolder, F. Rousseaux, V. Mathet, and H. Launois, *Science* **280** 1919-1922 (1998)

9. D. Weller, J.E.E. Baglin, A.J. Kellock, K.A. Hannibal, M.F. Toney, G. Kusinski, S. Lang, L. Folks, M.E.Best, and B.D. Terris, *J. Appl. Phys.* **87** 5768-5770 (2000)

10. W.M. Kaminsky, G.A.C. Jones, N.K. Patel, W.E. Booij, M.G. Blamire, S.M. Gardiner, Y.B. Xu, and J.A.C.Bland, *Appl. Phys. Lett.* **78** 1589-1591 (2001)

11. D. Ozkaya, R.M. Langford, W.L. Chan, and A.K. Petford-Long, *J. Appl. Phys.* **91** 9937-9942 (2002)

12. K. Zhang, R. Gupta, K.P. Lieb, Y. Luo, G.A. Muller, P. Schaaf, and M. Uhrmacher, *Eur. Phys. Lett.* **64** 668(2003)

13. K. Zhang, K.P. Lieb, G.A. Müller, P. Schaaf, M. Uhrmacher, M. Münzenberg, *Eur. Phys. J. B* **42** 193-204 (2004)

14. G.A. Müller, E. Carpene, R. Gupta, P. Schaaf, K. Zhang, and K.P. Lieb, *Eur. Phys. J. B* **48**, 449-462 (2005)

15. J. McCord, L. Schultz, and J. Fassbender, *Adv. Mater.* **20**, 2090-2093 (2008)

16. D. Oshima, T. Kato, S. Iwata, and S. Tsunashima, *IEEE Transactions on Magnetics* **49**, 3608-3611 (2013)

17. M. Trassinelli, V.E Gafton, M. Eddrief, V.H. Etgens, S. Hidki, E. Lacaze, E. Lamour, X. Luo, M. Marangolo, J. Mérot, C. Prigent, R. Reuschl, J.-P. Rozet, S. Steydli, D. Vernhet, *Nucl. Instrum. Methods B***317** (A) 154-158 (2013)

18. J.P. Singh, R.C. Srivastava, H.M. Agrawal, P. Chand, R. Kumar, *Current Applied Physics* **11**532–537 (2011)

19. J.P. Singh, R.C. Srivastava, H.M. Agrawal, R. Kumar, V.R. Reddy, A. Gupta, *Journal of Magnetism and Magnetic Materials* **322** 1701–1705 (2010)

20. J.P. Singh, R.C. Srivastava, H.M. Agrawal, R. Kumar, *Nucl. Instrum. Methods B* **268** 1422–1426 (2010)

21. M. Trassinelli, M. Marangolo, M. Eddrief, V. H. Etgens, V. Gafton, S. Hidki, E. Lacaze, E. Lamour, C. Prigent, J.P. Rozet, S. Steydli, Y. Zheng, D. Vernhet, *Applied Physics Letters* **104**, 081906 (2014)

22. O.F. Caltun, *Journal of Optoelectronics and Advanced Materials* **7** (2) 739 – 744 (2005)

23. G.Dascalu, G. Pompilian, G. Chazallon, O.F. Caltun, S. Gurlui, C. Focsa,*Applied Surface Science* **278** 38-42 (2013)

24. O. Caltun, M. Feder, C. J. Liu, *Journal of Optoelectronics and Advanced Materials***6**(3) 955 – 958 (2004)

25. B.D. Cullity, S.R. Stock, *"Elements of X-Ray Diffraction, 3rd Ed."*, Prentice-Hall Inc., p 167-171 (2001)

26. A. Gumberidze, M. Trassinelli, N. Adrouche, C. I. Szabo, P. Indelicato, F. Haranger, J. M. Isac, E. Lamour, E. O. Le Bigot, J. Merot, C. Prigent, J. P. Rozet, D. Vernhet, *Rev. Sci. Instrum.***81**, 033303 (2010)

27. J. F. Ziegler, J. P. Biersack, M. D. Ziegler, *"Stopping and Range of Ions in Matter"* (SRIM Company, 2008)

28. L. Panitzsch, M. Stalder, R.F. Wimmer-Schweingruber, *Rev. Sci.Instrum.***80**, 113302 (2009)

29. L. Panitzsch, M. Stalder, R.F. Wimmer-Schweingruber, *Rev. Sci. Instrum.***82**, 033302 (2011)

30. D. B. Chrisey, G. K. Hubler, *"Pulsed Laser Deposition of Thin Films"*John Willey & Sons, Inc. New York (1994)

31. R. B. van Dover, E. M. Gyorgy, S. Venzke, J. M. Philips, J. H. Marshall, R. J. Felder, R.M. Fleming, H. O'Bryan,*Jr. J. Appl. Phys.***75** 612 (1994)

32. I. Horcas, R. Fernandez, J.M. Gomez-Rodriguez, J. Colchero, J. Gomez-Herrero, A. M. Baro. s.l. : Rev. Sci. Instrum.**78**, 2007.

33. 89-1009 ICDD card (franklite)

34. B.D. Cullity, *"Elements of X-ray Diffraction"*, Addision-Weseley, New York (1972)

35. A.H. Morrish, X.Z. Zhou, G.C. Hadjipanayis, G.A. Prinz (Eds.) *"Plenum Press"*, New York (1991) 513–520

36. W. Wang, W. Widiyastuti, T. Ogi, I.W. Lenggoro, K. Okuyama,*Chem. Mater*. **19** 1723–1730 (2007)

37. S. Singh, N. Kumar, A. Jha, M. Sahni, R. Bhargava, A. Chawla, R. Chandra, S. Kumar, S. Chaubey. *J Supercond Nov Magn*, **27** 821–826 (2014).

38. L. Raghavan, G. Pookat, H. Thomas, S. Ojha, D.K. Avasthi, M.R. Anantharaman, *Journal of Magnetism and Magnetic Materials* **385,** 265–271 (2015)

39. A.A. Timopheev, A.M. Azevedo, N.A. Sobolev, K. Brachwitz, M. Lorenz,M. Ziese, P. Esquinazi, M. Grundmann*Thin Solid Films* **527** (2013) 273–277

40. S. Nakashima, K. Fujita, K. Tanaka, K. Hirao, T. Yamamoto, I. Tanaka, *PHYSICAL REVIEW B* **75** 2007.

41. J.P. Singh, G. Dixit, R.C. Srivastava, H. Kumar, H.M. Agrawal, R. Kumar, *Journal of Magnetism and Magnetic Materials* **324** 3306–3312 (2012)

42. S.N. Dolia, M.S. Dhawan, A.S. Prasad, S. Kumar, A. Samariya, R.K. Singhal, R. Kumar, *Radiat. Eff. Def. Solids* **166**, 558-563 (2011)

43. S.N. Dolia, P.K. Sharma, M.S. Dhawan, S. Kumar, A.S. Prasad, A. Samariya, S.P. Pareek, R.K. Singhal, K. Asokan, Y.T. Xing, M. Alzamora, and E. Saitovitach, *App. Surf. Sci.* **258**, 4207-4211 (2012)

44. S.N. Dolia, P.K. Sharma, A. Samariya, S.P. Pareek, A.S. Prasad, M.S. Dhawan, S. Kumar, K. Asokan, *Radiat. Eff. Def. Solids* **168**, 537-546 (2013)

45. S.N. Dolia, S.P. Pareek, A. Samariya, P.K. Sharma, A.S. Prasad, M.S. Dhawan, S. Kumar, K.B. Sharma, K. Asokan, *Radiat. Eff. Def. Solids* **168**, 525-531 (2013)

46. Y.D. Zhang, J. I. Budnick, W. A. Hines, C. L. Chien, J. Q. Xiao, *Applied Physics Letters* **72** 20-53 (1998)

47. A. Adair, J.T.E. Galindo, C. Botez, V.C. Flores, D.B. Baques, L.F. Cobas, J.A. Matutes-Aquino, *Materials Research Society Symposium Proceedings* **962** 10–18 (2007)

48. J. Wan, G. Tang, Y. Qian, *Applied Physics A* **86** (2) 261–264 (2007)

49. M. Atif, S.K. Hasanain, M. Nadeem, *Solid State Communications* **138**, Issue 8, 416–421 (2006)

50. L.D. Tung, V.Kolesnichenko, G. Caruntu, D. Caruntu, Y.Remond, V.O. Golub, C.J O'Connor, L. Spinu, *Physica B: Condensed Matter* **319**, Issues 1–4, 116–121 (2002)

51. J.F. Hochepied, J.F. Hochepied, P. Bonville, M. P. Pileni, *J. Phys. Chem. B* **104**, 905-912 (2000)

52. M. Yokoyama, E. Ohta, T. Sato, T. Komaba, *J. Phys. IV Fr.***7**, C1-521 (1997)

53. V.G. Vologin, V. D. Parkhomenko, S. F. Dubinin, Yu. G. Chukalkin, B. N. Goshchitskii, S. K. Sidorov, V. V. Petrov, *Phys. Status Solidi* A **33** K83 (1976)

Table 1.

Parameters estimated from X-ray diffractograms, from VSM measurements at room temperature and from SQUID measurements

	Angle [°]	**Fluence [ion/cm^2]** (± 50%)	***a*** **[Å]** (± 0.07**)**	***D*** **[nm]**	**AFM grain size [nm]** (± 1 nm**)**	**AFM R_{p-p} [nm]**	**Coercitivity**		**Volumic magnetization [emu/cm^3]**	**T_B [K]**
							Oe	**[kA/m]**		
PLD target			8.44	20 (± 0.3**)**						
P1		**pristine**	8.45	11 (± 0.2**)**	25	10	46	3.7	75	
	60	**3x10^{14}**	8.45	11 (± 0.2**)**			56	4.5	106	
P2		**pristine**	8.43	12 (± 0.2**)**	40	10	18	1.4	40	
	60	**3x10^{11}**	8.43	13 (± 0.8**)**			74	5.9	57	
P3		**pristine**	8.43	12 (± 0.2**)**	30	10	9	0.7	165	216
	60	**1x10^{14}**	8.43	13 (± 0.8**)**			5	0.4	195	226
P4		**pristine**	8.43	12 (± 0.2**)**	30	10	48	3.8	43	131
	60	**3x10^{14}**	8.43	16 (± 0.9**)**			61	4.9	45	139

Figure list

Figure 1 SRIM predictions on ion penetration and collision events in the present experimental conditions: $ZnFe_2O_4$ / Si (111) thin film (thickness - 250 nm) is irradiated by a Ne^{9+} ion beam (90 keV) at 60° incidence angle. Left: distribution of the ion penetration. Right: distribution of atom displacement in the sample.

Figure 2 Scheme of the collision chamber. The manipulator and different diagnostic tools are shown: the retractable Faraday cups array (FCA) and a CCD camera. The CCD camera detects the emitted radiation from the sample during the irradiation process under 30 ° angle relative to the sample surface

Figure 3SEM cross section of $ZnFe_2O_4$ – P1 thin film.

Figure 4 (a) (left) AFM image of the Zn ferrite P3 thin film at 500 nm x 500 nm scan surface; (right) Three-dimensional AFM image of zinc ferrite films deposited on Si (111) substrate showing a hilly morphology. (b) AFM image of the Zn ferrite P2, P3, P4 irradiated thin films at 500 nm x 500 nm scan surface

Figure 5Zoom of XRD spectra of pristine (annealed or not) and irradiated $ZnFe_2O_4$ - P3 sample with a step of 0.005°, and a speed of 1°/min, compared to PLD target (color online).

Figure 6 Magnetic hysteresis loops at 300 K for the pristine and irradiated P3 zinc ferrite thin films. The inset presents the variation of the coercivity of sample P3 induced by irradiation process (color online).

Figure 7 ZFC-FC dependence of magnetization for the pristine and irradiated zinc ferrite P3 thin films (color online).

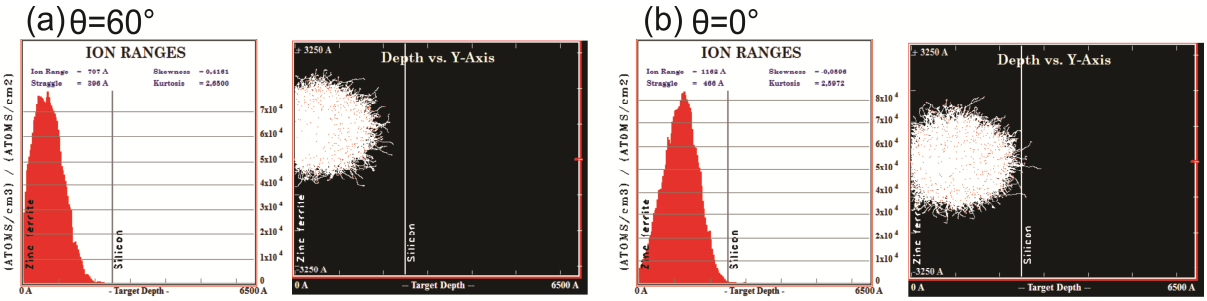

Fig. 1

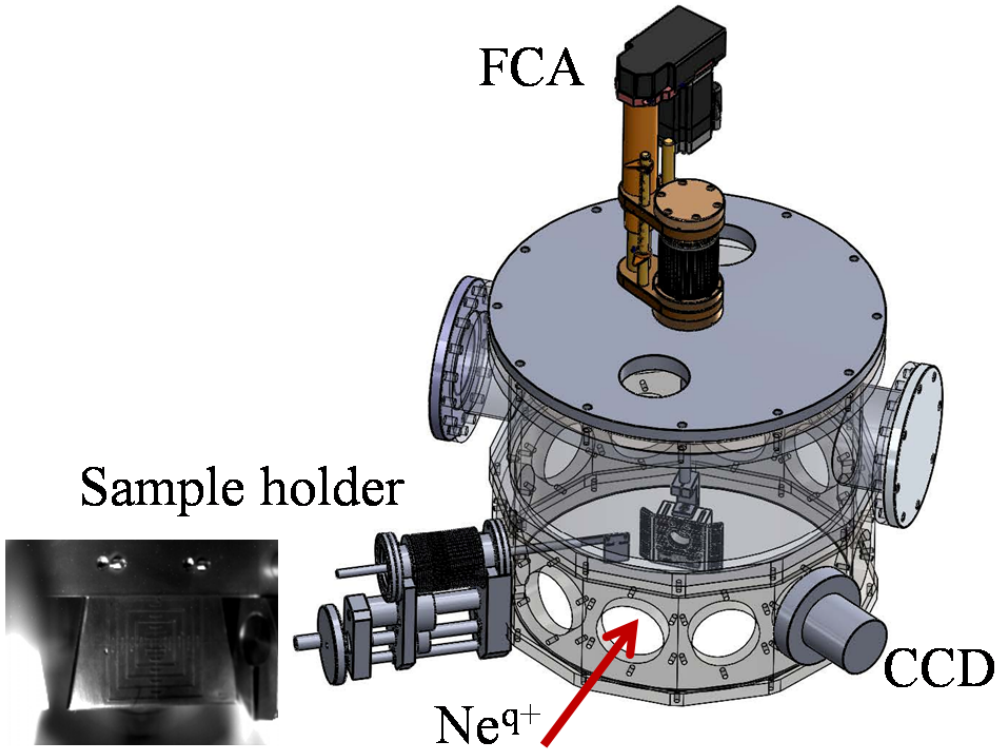

Fig. 2

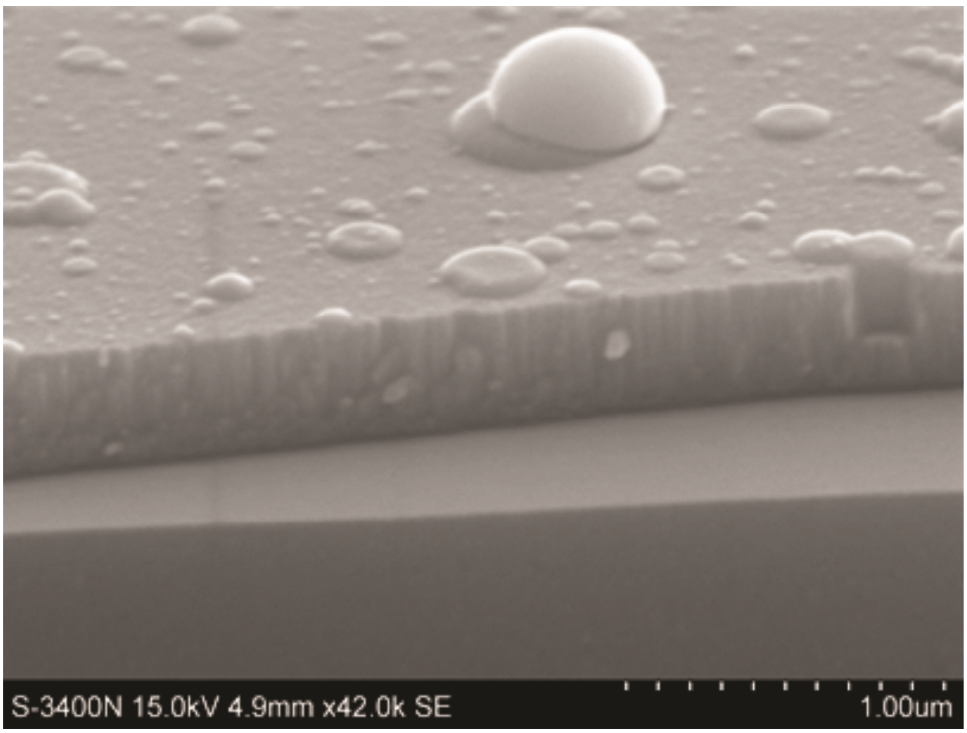

Fig. 3

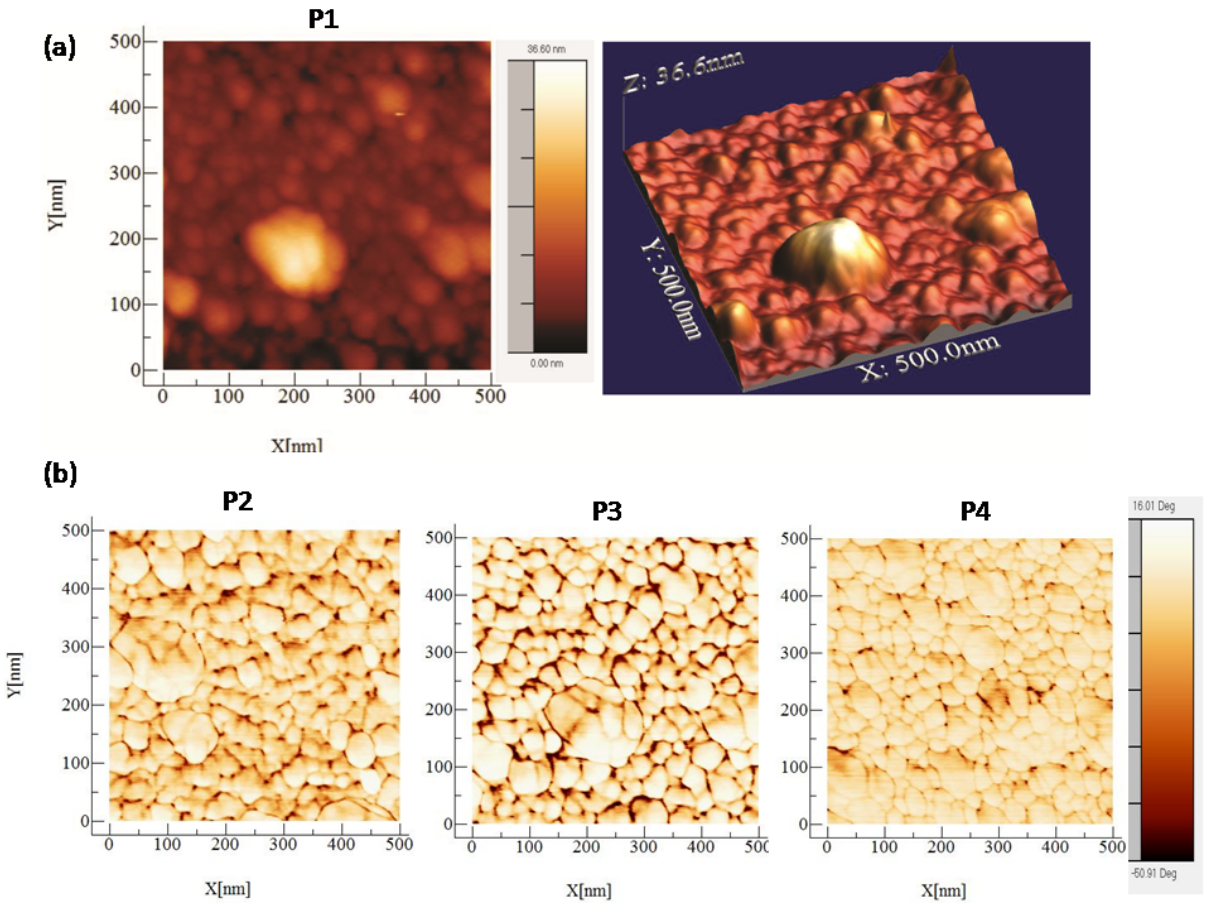

Fig. 4

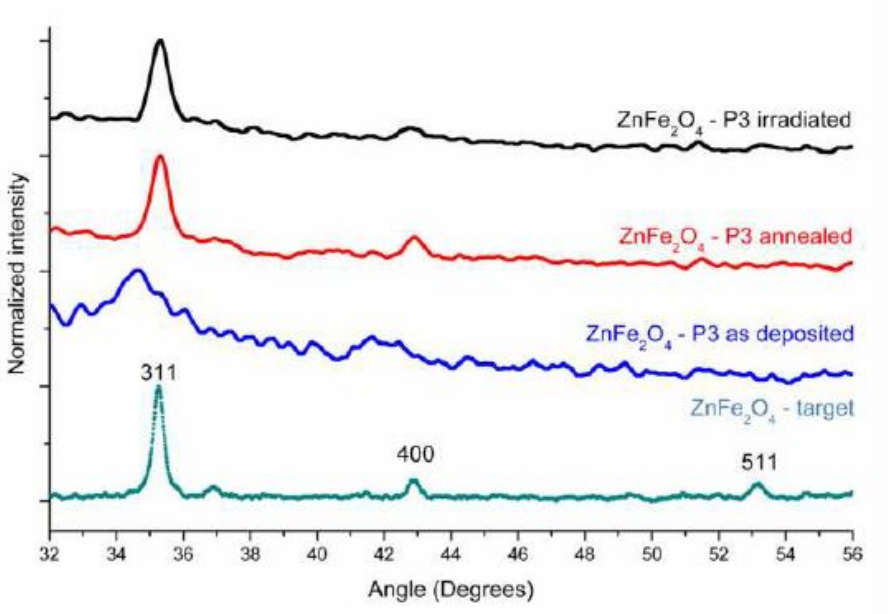

Fig. 5

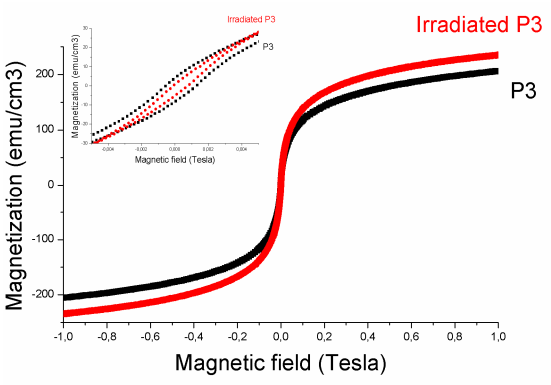

Fig. 6

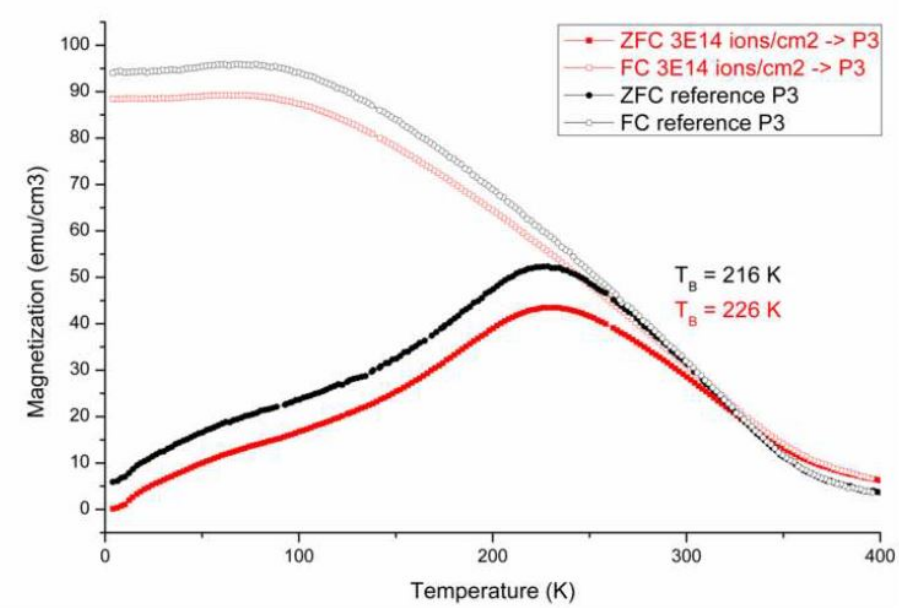

Fig. 7